Journal of Vibration Engineering & Technologies
https://doi.org/10.1007/s42417-024-01287-2

ORIGINAL PAPER

Free Vıbratıon of a Carbon Nanotube-Reınforced Nanowıre/Nanobeam wıth Movable Ends

Büşra Uzun[1] · **Mustafa Özgür Yaylı**[1]

Received: 29 November 2023 / Revised: 10 January 2024 / Accepted: 13 January 2024
© The Author(s) 2024

Abstract

Objective The purpose of this work is to investigate the size-dependent free vibrations of carbon nanotube-reinforced nanowires/nanobeams with movable ends. For this purpose, two movable end conditions are considered for carbon nanotube-reinforced nanowires/nanobeams with different carbon nanotube distributions. The size effect is addressed with the modified couple stress theory, which includes a material length scale parameter.

Methods In this study, a solution approach based on the Fourier sine series and Stokes' transformation is used. With the help of this approach, both rigid and movable end conditions can be investigated. Firstly, equation sets consisting of infinite series and movable end parameters are derived. Then, eigenvalue problems are obtained for the free vibration of carbon nanotube-reinforced nanowires/nanobeams. The eigenvalues of these problems give the frequencies of the carbon nanotube-reinforced nanowires/nanobeams with movable ends.

Conclusions The eigenvalue problems obtained in this study can be used to examine both rigid and movable end conditions. The accuracy of the problems obtained for solution is proven by various comparison studies. Then, a series of analyses are carried out for nanowire/nanobeam reinforced with carbon nanotubes, including both the size effect and the rotary inertia effect. When the frequencies of nanowire/nanobeams reinforced with carbon nanotubes are examined, it is understood that the material length scale parameter, carbon nanotube distribution, carbon nanotube volume fraction, rotational and lateral spring parameters can cause significant changes in free vibration.

Keywords Carbon nanotube-reinforced nanowires/nanobeams · Modified couple stress theory · Rotary inertia · Movable end · Free vibration

Introduction

Nanotechnology is usually regarded as a major branch in technological developments, given the ongoing progress in the increasing fulfillment of human requirements and technology through the use of diminutive instruments and materials. Nanowires/nanobeams (NWs/NBs) have found several applications in a wide range of nano industries, including manufacturing, oscillators, pharmaceuticals, electronics, clocks, healthcare, space research, aircraft technology, environmental protection, energy sectors, sensors, numerous engineering constructions and biomedical sectors [1]. By comparing the findings of the theoretical results with experimental studies, it is possible to obtain the mechanical and dynamical properties of these structures and machines. It is appropriate to define the mechanical and dynamic response of nanomechanical systems.

In recent years, some strength enhancement methods using carbon nanotubes (CNTs) have been tried to increase the theoretical and experimental strength of micro/nanobeams. Sometimes the main reason for these strength increases is to control the vibration frequencies or to keep the micro or nanoscale beam displacement at a certain point. It is also aimed to increase the critical buckling loads in slender elements. Esen et al. [2] used the Navier method to show the dynamic of functionally graded carbon nanotube-reinforced (CNTR) shear deformable beams. Mahmoodi et al. [3] modelled an experimental and theoretical analysis for nonlinear vibration behavior of a viscoelastic composite CNTR cantilever beam. Lin and Xiang [4] studied the

✉ Büşra Uzun
buzun@uludag.edu.tr

Mustafa Özgür Yaylı
ozguryayli@uludag.edu.tr

[1] Department of Civil Engineering, Bursa Uludag University, Engineering Faculty, Görükle Campus, 16059 Bursa, Turkey

Published online: 13 March 2024

dynamics of the two types of composite carbon nanotube-reinforced beam utilizing the different beam theories. The dynamics of composite carbon nanotube-reinforced Timoshenko beams affected by waviness, agglomeration, distribution and length of CNTs was studied by Heshmati et al. [5]. Rafiee et al. [6] studied the dynamic response of piezoelectric CNTR composite beams with multiple scale solutions. Zhang et al. [7] employed content-dependent nonlinearity to investigate the dynamic response of carbon nanotube-reinforced plates. Özdemir et al. [8] studied the thermal vibration of rotating CNTR composites via Timoshenko beam theory and finite element method. The thermal vibration characteristics of CNT-reinforced coupled beam systems were presented by Ghandehari et al. [9]. Bondla et al. [10] conducted a novel fuzzy finite element method to caculate the frequencies of CNTR panels. Thermoelastic deflection and frequency analyses of CNTR sandwich structures were studied by Maher et al. [11, 12]. In addition, Maher et al. [13] presented a numerical approach with experimental validation for the CNTR sandwich structure. Esen et al. [14] showed the dynamic of CNTR beams under the effect of a moving mass. Wattanasakulpong and Ungbhakorn [15] proposed analytical solutions of embedded CNTR beams for three different responses. Ke et al. [16], Wu et al. [17] and Alimoradzadeh and Akbas [18] examined the nonlinear vibration of CNTR beams. Maher et al. [19] showed both theoretical and exprerimental examinations of the vibration of CNTR composites. Also, we can encounter review studies [20, 21] of the CNTR composites in the literature.

Conducting experiments at the nanoscale and compiling the results are very difficult. It is also very expensive to obtain samples to be used in experiments at this size. Theoretical studies are becoming more prominent to reduce the losses in the samples in case of a possible contrary situation. The fact that classical elasticity theory does not include a size parameter suggests that it is not as effective as desired at small sizes. To consider the small size dependency, several size-dependent elasticity theories such as modified couple stress theory (MCST) of Yang et al. [22], Eringen's nonlocal theory [23], couple stress theory [24, 25], doublet mechanics theory [26, 27], the strain gradient higher order model of Lam et al. [28] and nonlocal strain gradient theory of Lim et al. [29] were introduced. Ersoy et al. [30] presented the dynamic CNTs with rotary inertia and modified couple stress effects. Togun and Bağdatlı [31] proposed the nonlinear vibration of tensioned nanobeam based on the MCST. The dynamics of Timoshenko CNTs were studied via doublet mechanics in Refs. [32, 33]. Gül and Aydoğdu [34] proposed a smal-scale Timoshenko–Ehrenfest beam model for doublet mechanics-dependent analyses. Timoshenko microbeam vibration was studied by Awrejcewicz et al. [35] and Esen [36] via MCST. Small size and crack effects for the functionally graded beams were investigated in Refs. [37, 38]. Also, the nonlocal strain gradient theory was used to analyze the various structures such as perforated nanobeams [39–41], nano/micro-capillary systems [42, 43], functionally graded nanoplate [44], etc. In recent years, we can see the various analyses of CNTR small-scale beams. Civalek et al. [45] presented the MCST-based vibration of CNTR microbeams via the Navier solution. Alimoradzadeh et al. [46] showed the nonlinear dynamics of CNTR micro scale beam with non-uniform cross section via the Euler-Bernoulli beam (EBB) theory and MCST. Abdelrahman et al. [47] and Esen et al. [48] presented the nonlocal strain gradient dynamic of CNTR nanobeams affected by moving point load. Daikh et al. [49, 50] proposed the nonlocal strain gradient effects on the CNTR nanoplates and nanobeam, respectively. Borjalilou et al. [51] defined the exact nonlocal solutions of CNTR nanobeams. Taati et al. [52] presented the nonlinear vibration of CNTR nanobeams via the perturbation technique and nonlocal elasticity. With the development of computer memory and the chip industry in the coming decades, the importance of this valuable theoretical and experimental work will be much better understood. Unpredictable size effects cannot be explained solely by the theory used, but it is clear that a size effect cannot be ruled out.

As mentioned before, nanobeam models of carbon nanotubes and matrix structures reinforced with carbon nanotubes have attracted attention. Determining the mechanical responses of nanowire/nanobeam elements, which are widely used in nano/micro-electromechanical systems structures, is very important as it occurs at a precise size. This study is unique because it can analyze a situation that can be encountered in a realistic application. This study can calculate the vibration frequencies of carbon nanotube-reinforced nanowires/nanobeams (CNTR-NWs/NBs) with non-idealized movable boundary conditions as well as idealized boundaries such as simply supported (SS) and clamped support (CC) cases and free end, which we frequently encounter in the literature, with the size effect. It is too difficult to apply idealized boundary conditions in practice, and very small moves occur at the boundaries. This study aims to provide guidance in predicting the frequencies of CNTR nanobeam structures subjected to vibration movement. In this study, the free vibration response of CNTR-NWs/NBs exposed to deformable boundary conditions is studied. Stokes' transformation with the Fourier series are employed to construct eigenvalue problems which include the effects of elastic lateral and rotational springs. The volume fraction of carbon nanotube is defined using four different distributions. Various parameters are explored in this work by giving proper values to elastic spring parameters at the ends. The accuracy and validity of the present method are validated by comparing the calculated results with those in the literature.

Modified Couple Stress Theory-Based Vibration

As mentioned in the first part of the article, higher-order elasticity theories have been frequently preferred in the analysis of small-scale nanowire and nanobeam structures.

MCST [22], which is one of the higher-order elasticity theories, is one of the key points of this study. In this study, the free vibration analysis of CNTR-NWs/NBs with movable ends is investigated based on MCST. The equation of motion is derived with the help of Hamilton's principle with the following expression:

$$\int_{t_1}^{t_2} (\delta T - \delta S + \delta W)dt = 0. \tag{1}$$

Here, t_1 and t_2 represent the start and end time of the motion, respectively, while t is time, T, S and W are the kinetic energy, strain energy and work done by external loads, respectively. δ is the variation operator. In this study, $W = 0$ is taken, since free vibration analysis will be performed and the focus will be on the reinforcement of CNT, movable boundaries and the size effect of MCST. The well-known kinetic energy expression is written as follows:

$$T = \frac{1}{2}\int_{\Xi} \rho\left[\left(\partial_t u_1\right)^2 + \left(\partial_t u_2\right)^2 + \left(\partial_t u_3\right)^2\right]d\Xi. \tag{2}$$

In Eq. (2), Ξ is the volume occupied by the material, while ρ is the mass density of the material. ∂_t means taking the derivative once with respect to t ($\partial_t = \partial/\partial t$). u_1, u_2 and u_3 denote the displacements in the x, y and z directions, respectively, and are expressed as follows [30]:

$$u_1(x,z,t) = -z\partial_x v(x,t); u_2(x,z,t) = 0; u_3(x,z,t) = v(x,t). \tag{3}$$

The expressions in Eq. (3) are the displacements defined on the basis of the Euler–Bernoulli beam theory. EBB theory is the fundamental beam theory and gives good results in the analysis of bending elements with a high aspect ratio (L/h). When rotary inertia effects are considered in the vibration responses analyzed with the EBB theory, it is called the Rayleigh beam (RB) theory. Here, $v(x,t)$ is the lateral displacement of NW/NB. ∂_x means taking the derivative once with respect to $x\left(\partial_x = \partial/\partial x\right)$. With the displacement fields given above, the kinetic energy expression is rewritten as follows:

$$T = \frac{1}{2}\int_0^L \left[m_0\left(\partial_t v(x,t)\right)^2 + m_2\left(\partial_{xt} v(x,t)\right)^2\right]dx. \tag{4}$$

In Eq. (4), ∂_{xt} means taking the derivative of the expression in which it appears once with respect to both x and t ($\partial_{xt} = \partial/\partial x\partial t$). L is the length of the NW/NB, while m_0 and m_2 are the mass moments of inertia. For a homogeneous NW/NB, $m_0 = \rho A$ and $m_2 = \rho I$. Here, A is the cross-sectional area and I is the moment of inertia. In the MCST proposed by Yang et al. [22] to analyze small-scale materials and structures, the strain energy is defined as follows:

$$S = \frac{1}{2}\int_{\Xi} \left(\sigma_{ij}\epsilon_{ij} + \psi_{ij}\chi_{ij}\right)d\Xi. \tag{5}$$

In the strain energy, σ_{ij},$\in_{ij}$, ψ_{ij} and χ_{ij} are the stress tensor, strain tensor, deviatoric part of the couple stress tensor and the rotation gradient tensor, respectively. These tensors are defined as follows [22]:

$$\in_{ij} = \frac{1}{2}\left(\partial_j u_i + \partial_i u_j\right), \tag{6}$$

$$\sigma_{ij} = E \in_{ij}, \tag{7}$$

$$\psi_{ij} = 2Gl^2\chi_{ij}, \tag{8}$$

$$\chi_{ij} = \frac{1}{2}\left(\partial_j \Omega_i + \partial_i \Omega_j\right). \tag{9}$$

In the above expressions, E is the modulus of elasticity, G is the shear modulus, l is the material length scale parameter and Ω is the rotation vector. The rotation vector Ω is written as follows:

$$\Omega_i = \frac{1}{2}\left(e_{ijk}\partial_j u_k\right). \tag{10}$$

Here, e_{ijk} specifies the permutation symbol.

Material Properties of CNTR Composites

In this study, carbon nanotube-reinforced composite NWs/NBs are analyzed. In this section, the effective material properties of CNTR composites are introduced. Different techniques have been developed by experts to evaluate the properties of composite materials. We can list some of these techniques as follows: the rule of mixture [14, 15, 53], Halpin–Tsai model [54, 55], Hui–Shia model [54] and Mori–Tanaka approach [56, 57]. The mentioned models describe the microstructural properties of the material and the interactions between phases in different ways. The rule of mixture is widely used in unidirectional fiber-reinforced composites, while the Halpin–Tsai model describes the material properties for particulate composites and the Mori–Tanaka can be used to calculate the elastic modulus of both aligned and randomly oriented CNTR composites [19]. Figure 1 shows the cross-sectional views of composite NWs/NBs composed of carbon nanotube-reinforced polymethyl methacrylate (PMMA) matrix with CNT distributions in various forms. In this study, four different distributions are adopted as can be seen from the figure. These are: composite with ◇ shaped carbon nanotube distribution (CNTR-◇), composite with homogeneous carbon nanotube distribution along the height (CNTR-□), composite with X-shaped carbon nanotube distribution (CNTR-X) and composite with ▽ shaped carbon nanotube distribution (CNTR-▽). As can be understood, in the CNTR

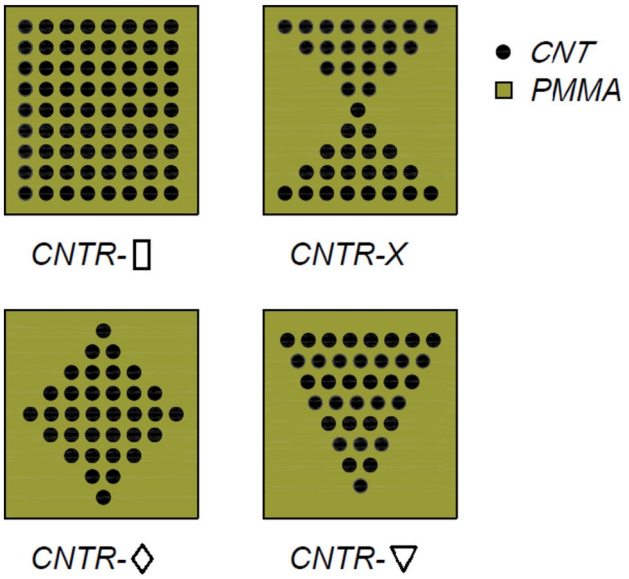


Fig. 1 View of cross sections of CNTR composites

beam structure to be examined in this study, the CNTs are distributed in the same direction within the matrix. For this reason, in this study, the rule of mixture is used. The following formulations are presented to describe the effective material properties of the reinforced composite NWs/NBs depending on the properties of the CNT and PMMA matrix [15]:

$$E_{11}^{\mathrm{CNTR}}(\bar{z}) = \eta_1 \Xi_{\mathrm{CNT}}(\bar{z}) E_{11}^{\mathrm{CNT}} + \Xi_{\mathrm{PMMA}}(\bar{z}) E^{\mathrm{PMMA}}, \tag{11}$$

$$\nu^{\mathrm{CNTR}}(\bar{z}) = \Xi_{\mathrm{CNT}}(\bar{z}) \nu^{\mathrm{CNT}} + \Xi_{\mathrm{PMMA}}(\bar{z}) \nu^{\mathrm{PMMA}}, \tag{12}$$

$$\rho^{\mathrm{CNTR}}(\bar{z}) = \Xi_{\mathrm{CNT}}(\bar{z}) \rho^{\mathrm{CNT}} + \Xi_{\mathrm{PMMA}}(\bar{z}) \rho^{\mathrm{PMMA}}, \tag{13}$$

$$\frac{\eta_2}{E_{22}^{\mathrm{CNTR}}(\bar{z})} = \frac{\Xi_{\mathrm{CNT}}(\bar{z})}{E_{22}^{\mathrm{CNT}}} + \frac{\Xi_{\mathrm{PMMA}}(\bar{z})}{E^{\mathrm{PMMA}}}, \tag{14}$$

$$\frac{\eta_3}{G_{12}^{\mathrm{CNTR}}(\bar{z})} = \frac{\Xi_{\mathrm{CNT}}(\bar{z})}{G_{12}^{\mathrm{CNT}}} + \frac{\Xi_{\mathrm{PMMA}}(\bar{z})}{G^{\mathrm{PMMA}}}, \tag{15}$$

$$\Xi_{\mathrm{CNT}} + \Xi_{\mathrm{PMMA}} = 1. \tag{16}$$

Here, E_{11}^{CNT}, E_{22}^{CNT}, G_{12}^{CNT}, ν^{CNT} and ρ^{CNT} indicate the elastic modulus, shear modulus, Poisson's ratio, and mass density of the carbon nanotube, respectively. Similarly, E^{PMMA}, G^{PMMA}, ν^{PMMA} and ρ^{PMMA} refer to the elastic modulus, shear modulus, Poisson's ratio and mass density of the PMMA matrix, respectively. Finally, Ξ_{CNT} and Ξ_{PMMA} refer to the volume fractions of the carbon nanotube and PMMA matrix. The coefficients expressed as η_1, η_2, η_3 are called carbon nanotube efficiency parameters and are calculated as follows [15]:

$$\text{for} \Xi_{\mathrm{CNT}}^{*} = 0.12 : \eta_1 = 1.2833, \eta_2 = \eta_3 = 1.0556, \tag{17}$$

$$\text{for} \Xi_{\mathrm{CNT}}^{*} = 0.17 : \eta_1 = 1.3414, \eta_2 = \eta_3 = 1.7101, \tag{18}$$

$$\text{for} \Xi_{\mathrm{CNT}}^{*} = 0.28 : \eta_1 = 1.3238, \eta_2 = \eta_3 = 1.7380. \tag{19}$$

Additionally, the following correlations are calculated between Ξ_{CNT}^{*} and Ξ_{CNT} for four different reinforcement distributions to be analyzed [15]:

$$\mathrm{CNTR}-\square : \quad \Xi_{\mathrm{CNT}}(\bar{z}) = \Xi_{\mathrm{CNT}}^{*}, \tag{20}$$

$$\mathrm{CNTR}-X : \quad \Xi_{\mathrm{CNT}}(\bar{z}) = 4\frac{|\bar{z}|}{h}\Xi_{\mathrm{CNT}}^{*}, \tag{21}$$

$$\mathrm{CNTR}-\square : \quad \Xi_{\mathrm{CNT}}(\bar{z}) = 2\left(1 - \frac{2|\bar{z}|}{h}\right)\Xi_{\mathrm{CNT},}^{*} \tag{22}$$

$$\mathrm{CNTR}-\nabla : \quad \Xi_{\mathrm{CNT}}(\bar{z}) = \left(1 + \frac{2\bar{z}}{h}\right)\Xi_{\mathrm{CNT}}^{*}. \tag{23}$$

The calculation of Ξ_{CNT}^{*} seen in the equations is done as follows [15]:

$$\Xi_{\mathrm{CNT}}^{*} = \frac{M_{\mathrm{CNT}}}{M_{\mathrm{CNT}} + \left(\frac{\rho_{\mathrm{CNT}}}{\rho_{\mathrm{PMMA}}}\right) - \left(\frac{\rho_{\mathrm{CNT}}}{\rho_{\mathrm{PMMA}}}\right)M_{\mathrm{CNT}}}. \tag{24}$$

Here, M_{CNT} denotes the mass fraction of the carbon nanotube. As can be seen from Fig. 1, three of the CNTR-NW/NB sections (CNTR-◇, CNTR-□, CNTR-X) are symmetrical with respect to the middle axis. The symmetry mentioned in another one (CNTR-▽) is not present. The non-symmetrical situation results in the geometric axis and neutral axis being in different places in CNTR-▽. This situation requires the inclusion of axial displacements in the problem. As can be seen from Eq. (3), axial displacements are not taken into account in the expressions written for CNTR-NWs/NBs and only lateral displacements are considered. In formulations to be established based on lateral displacements, axial displacements do not need to be taken into account by calculating the location of the neutral axis and including it in the processes, because both solutions give the same results. In this study, solutions will be realized using the neutral axis set. It should be noted again that there is no need to use the neutral axis set for CNTR-◇, CNTR-□ and CNTR-X. The formula that we can frequently encounter for functionally graded

composite beams is expressed as follows for CNTR-NW/NB [52]:

$$\Gamma = \frac{D_1}{D_2}. \tag{25}$$

Here, Γ defines the distance between the central axis and the neutral axis, and D_1 and D_2 are written as follows:

$$D_1 = \int_{-h/2}^{+h/2} Q_{11}^{\mathrm{CNTR}}(\bar{z})\bar{z}d\bar{z}, \tag{26a}$$

$$D_2 = \int_{-h/2}^{+h/2} Q_{11}^{\mathrm{CNTR}}(\bar{z})d\bar{z}. \tag{26b}$$

Here, $Q_{11}^{\mathrm{CNTR}}(\bar{z})$ is defined by:

$$Q_{11}^{\mathrm{CNTR}}(\bar{z}) = \frac{E_{11}^{\mathrm{CNTR}}(\bar{z})}{1-\nu^{\mathrm{CNTR}}(\bar{z})^2}. \tag{27}$$

Vibration for CNTR-NW/NB

In the previous sections, the theoretical background of the MCST and the relations of the material properties of CNTR composites are given. Now, the derivation of the free vibration equation for CNTR-NWs/NBs is shown. In their study, Ersoy et al. [30] presented equations based on MCST and Rayleigh beam theory for beams with constant material properties. In this study, the expressions presented in the article by Ersoy et al. [30] are adapted for CNTR-NW/NB. The expressions introduced in Eqs. (6–9) are derived for the CNTR-NW/NB by utilizing the displacements written for the Euler–Bernoulli NW/NBs as follows [30]:

$$\in_{xx} = -z\partial_{xx}v(x,t), \tag{28}$$

$$\sigma_{xx} = -E_{11}^{\mathrm{CNTR}}(z)z\partial_{xx}v(x,t), \tag{29}$$

$$\chi_{xy} = \chi_{yx} = -\frac{1}{2}\partial_{xx}v(x,t), \tag{30}$$

$$\psi_{xy} = \psi_{yx} = -G_{12}^{\mathrm{CNTR}}(z)l^2\partial_{xx}v(x,t). \tag{31}$$

It should be noted that only non-zero components are written above. The kinetic energy and strain energy expressions for CNTR- NW/NB based on MCST with non-zero components are derived as follows [30]:

$$T = \frac{1}{2}\int_0^L \left[M_0\left(\partial_t v(x,t)\right)^2 + M_2\left(\partial_t v(x,t)\right)^2\right]dx, \tag{32}$$

$$S = \frac{1}{2}\int_0^L \left(\kappa_{11} + \kappa_{55}l^2\right)\left(\partial_{xx}v(x,t)\right)^2 dx. \tag{33}$$

In the above expressions, M_0 and M_2 are the mass moments of inertia of the CNTR-NW/NB, while κ_{11} and κ_{55} are the bending and shear stiffnesses of CNTR-NW/NB, respectively. Based on the neutral axis set, these expressions for CNTR-NW/NB are defined as follows:

$$\kappa_{11} = b\int_{-\frac{h}{2}-\Gamma}^{+\frac{h}{2}-\Gamma} Q_{11}^{\mathrm{CNTR}}(z)z^2dz, \tag{34}$$

$$\kappa_{55} = b\int_{-\frac{h}{2}-\Gamma}^{+\frac{h}{2}-\Gamma} G_{12}^{\mathrm{CNTR}}(z)dz, \tag{35}$$

$$M_0 = b\int_{-\frac{h}{2}-\Gamma}^{+\frac{h}{2}-\Gamma} \rho^{\mathrm{CNTR}}(z)dz, \tag{36}$$

$$M_2 = b\int_{-\frac{h}{2}-\Gamma}^{+\frac{h}{2}-\Gamma} \rho^{\mathrm{CNTR}}(z)z^2dz. \tag{37}$$

The limits of the above integrals are written with respect to the position of the neutral axis indicated in Fig. 2. If the first variations of the kinetic energy and strain energy written in Eqs. (32 and 33) are written in Eq. (1), the expression in the double integral is found as follows and this gives us the free vibration equation [30]:

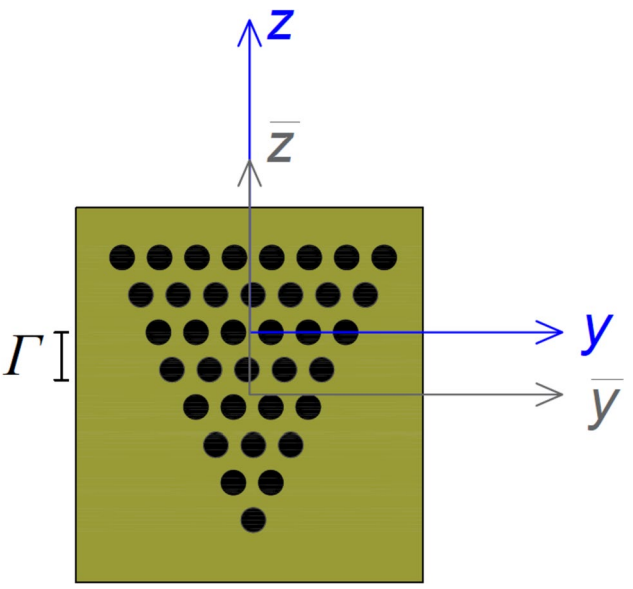


Fig. 2 View of neutral and geometrical axes for CNTR-▽ composites

$$\kappa_{11}\partial_{xxxx}v(x,t)+\kappa_{55}l^2\partial_{xxxx}v(x,t)+M_0\partial_{tt}v(x,t)-M_2\partial_{xxtt}v(x,t)=0. \tag{38}$$

Again using Hamilton's principle, the moment and shear force expressions are found as follows [30]:

$$V=M_2\partial_{xtt}v(x,t)-\kappa_{11}\partial_{xxx}v(x,t)-\kappa_{55}l^2\partial_{xxx}v(x,t), \tag{39}$$

$$M_b=-\kappa_{11}\partial_{xx}v(x,t)-\kappa_{55}l^2\partial_{xx}v(x,t). \tag{40}$$

Equation (39) indicates the shear force (V), while Eq. (40) indicates the bending moment (M_b). Taking $l=0$ in the above expressions degenerates the formulations to classical theory, which is independent of the size effect.

Stokes' Transform-Based Solution

In this study, the free vibration of CNTR-NWs/NBs with movable boundary conditions represented by Figs. 3 and 4 is analyzed according to MCST. One of the most important contributions of this study is to obtain a single solution that can also analyze movable boundary conditions. As encountered in the literature, if the boundary conditions change, a new solution is required. With the approach presented in this paper, it is not necessary to re-solve each time, but only by changing the parameters, i.e., by giving different stiffness values to the spring parameters, it is possible to change the boundary conditions at the same time. Noteworthy is the possibility of using nanowires/nanobeams as an atomic force microscope. The atomic force microscope's vibrational behavior may be impacted by nanoscale samples acting as masses that are connected to the testing apparatus via a linear spring during an experiment. To increase the sensitivity of the applied tests, it is sometimes not appropriate to have rigid boundary conditions. In this case, this method is considered so that the test results do not change too much for small stiffness losses. Equation (38) can be rewritten by applying the separation of variables technique ($v(x,t)=\lambda(x)e^{i\omega t}$) as follows:

$$\kappa_{11}d_{xxxx}\lambda(x)+\kappa_{55}l^2d_{xxxx}\lambda(x)-\omega^2M_0\lambda(x)+\omega^2M_2d_{xx}\lambda(x)=0. \tag{41}$$

Above, the partial differential equation in Eq. (38) is transformed into an ordinary differential equation by applying the separation of variables technique. Here, $\lambda(x)$ is the lateral displacement function, ω is the circular vibration and d's represent the first, second, third, etc. derivatives with respect to x along the beam. In this study, the mode shapes are assumed to be harmonically distributed and the Fourier sine series is adopted to define the displacement function [58–61].

$$\lambda(x)=\sum_{n=1}^{\infty}\zeta_n sin(\mu x),0<x<L. \tag{42}$$

In this study, the lateral displacement function $\lambda(x)$ is defined as a Fourier infinite function given above. In the

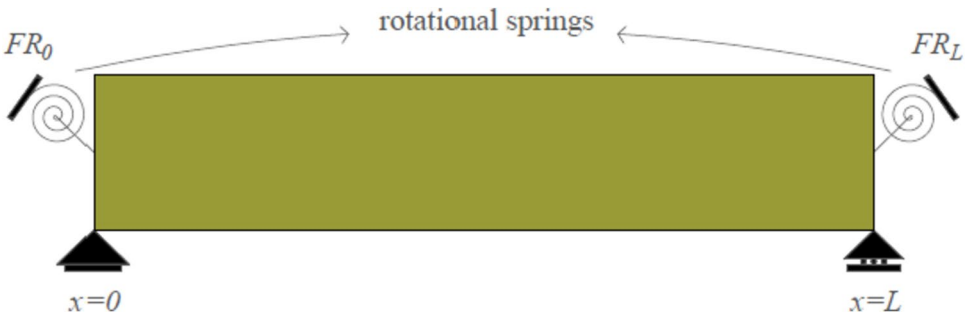


Fig. 3 CNT-reinforced composite NW/NB with rotational springs

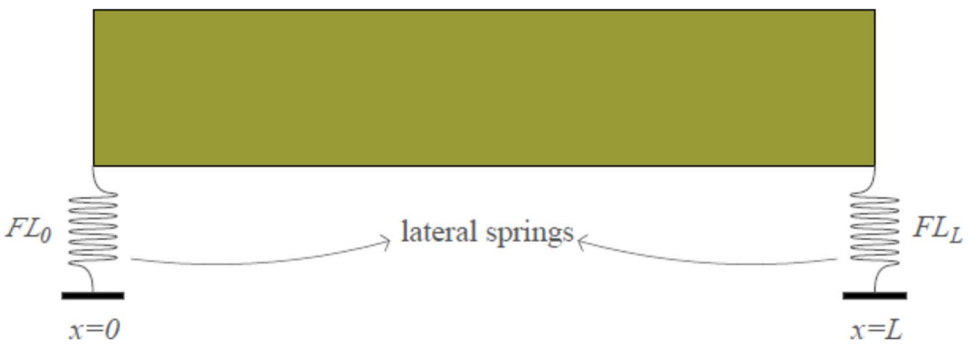


Fig. 4 CNT-reinforced composite NW/NB with lateral springs

function, ζ_n specifies the unknown Fourier coefficient and $\mu = n\pi/L$. As can be seen, this function is described for a region of nanowire/nanobeam and the end points (left end and right end) are excluded. The lateral displacement function is defined by $\lambda(x) = \lambda_0$ for the left end ($x = 0$) and it is described by $\lambda(x) = \lambda_L$ for the right end ($x = L$). In this study, two different movable boundary conditions are considered. For this reason, two different ζ_n are derived for rotationally restrained CNTR-NW/NB (Fig. 3) and laterally restrained CNTR- NW/NB (Fig. 4). Then, the Stokes' transformation is applied to force the boundary conditions to be satisfied. This method has been used by researchers to investigate the various analyses of many elements such as beam [58], nanobeam [59], FG porous microbeam [60] and nanotube [61]. However, in this study, it will be used for the first time for the effects of MCST and rotary inertia on the CNTR-NWs/NBs. We write the first four derivatives of the lateral displacement function from the articles using the mentioned method as follows [58]:

$$d_x\lambda(x) = \frac{\lambda_L - \lambda_0}{L} + \sum_{n=1}^{\infty}\left(\frac{2\Pi_1}{L} + \mu\zeta_n\right)cos(\mu x), \tag{43}$$

$$d_{xx}\lambda(x) = -\sum_{n=1}^{\infty}\mu\left(\frac{2\Pi_1}{L} + \mu\zeta_n\right)sin(\mu x), \tag{44}$$

$$d_{xxx}\lambda(x) = \frac{\lambda_L'' - \lambda_0''}{L} + \sum_{n=1}^{\infty}\left(\frac{2\Pi_2}{L} - \mu^2\left(\frac{2\Pi_1}{L} + \mu\zeta_n\right)\right)cos(\mu x), \tag{45}$$

$$d_{xxxx}\lambda(x) = -\sum_{n=1}^{\infty}\mu\left(\frac{2\Pi_2}{L} - \mu^2\left(\frac{2\Pi_1}{L} + \mu\zeta_n\right)\right)sin(\mu x). \tag{46}$$

Here, Π_1 and Π_2 are defined by:

$$\Pi_1 = (-1)^n\lambda_L - \lambda_0, \tag{47a}$$

$$\Pi_2 = (-1)^n\lambda_L'' - \lambda_0''. \tag{47b}$$

If the function λ(x) itself and its necessary derivatives are substituted in Eq. (41):

$$\sum_{n=1}^{\infty}\left[\left(\kappa_{11} + \kappa_{55}l^2\right)\left(-\mu\left(\frac{2\Pi_2}{L} - \mu^2\left(\frac{2\Pi_1}{L} + \mu\zeta_n\right)\right)\right) + \left(\omega^2 M_2\right)\left(-\mu\left(\frac{2\Pi_1}{L} + \mu\zeta_n\right)\right) - \left(\omega^2 M_0\right)\zeta_n\right]sin(\mu x) = 0 \tag{48}$$

is obtained. Solving the above equation gives a total Fourier coefficient depending on λ_0, λ_L, λ_0'' and λ_L''. In this total Fourier coefficient, the Fourier coefficient ζ_n^{RRNWB} of rotationally restrained CNTR-NW/NB is obtained by setting λ_0 and λ_L equal to zero, and the Fourier coefficient ζ_n^{TTNWB} of laterally restrained CNTR-NW/NB is obtained by setting λ_0'' and λ_L'' equal to zero as follows:

$$\zeta_n^{\mathrm{RRNWB}} = -\frac{2L^2 n\pi\left(\kappa_{11} + \kappa_{55}l^2\right)\left(\lambda_0'' - (-1)^n\lambda_L''\right)}{\left(\kappa_{11} + \kappa_{55}l^2\right)n^4\pi^4 - L^2\left(L^2M_0 + n^2\pi^2M_2\right)\omega^2}, \tag{49}$$

$$\zeta_n^{\mathrm{TTNWB}} = \frac{2n\pi\left(-L^2M_2\omega^2 + n^2\pi^2\left(\kappa_{11} + \kappa_{55}l^2\right)\right)\left(\lambda_0 - (-1)^n\lambda_L\right)}{\left(\kappa_{11} + \kappa_{55}l^2\right)n^4\pi^4 - L^2\left(L^2M_0 + n^2\pi^2M_2\right)\omega^2}. \tag{50}$$

The above Fourier coefficients are used for CNTR-NWs/NBs considered on the basis of MCST. If the material length scale parameters are neglected in these expressions, the Fourier coefficients that can be used for rotationally and laterally restrained carbon nanotube-reinforced classical wire/beam are obtained as follows:

$$\zeta_n^{\mathrm{RRCWB}} = -\frac{2L^2 n\pi\kappa_{11}\left(\lambda_0'' - (-1)^n\lambda_L''\right)}{\kappa_{11}n^4\pi^4 - L^2\left(L^2M_0 + n^2\pi^2M_2\right)\omega^2}, \tag{51}$$

$$\zeta_n^{\mathrm{TTCWB}} = \frac{2n\pi\left(-L^2M_2\omega^2 + n^2\pi^2\kappa_{11}\right)\left(\lambda_0 - (-1)^n\lambda_L\right)}{\kappa_{11}n^4\pi^4 - L^2\left(L^2M_0 + n^2\pi^2M_2\right)\omega^2}. \tag{52}$$

With the help of the governing equation and the derivatives given in Eqs. (43–46), the Fourier coefficients of laterally restrained and rotationally restrained CNTR-NWs/NBs are found. Now, the force boundary conditions are written and the eigenvalue problems are obtained. For the CNTR-NW/NB given in Fig. 3, the moment-dependent force boundary conditions are expressed as follows:

$$-\kappa_{11}\partial_{xx}v(x,t) - \kappa_{55}l^2\partial_{xx}v(x,t)|_{x=0} = -\mathrm{F}R_0 d_x\lambda_0, \tag{53}$$

$$-\kappa_{11}\partial_{xx}v(x,t) - \kappa_{55}l^2\partial_{xx}v(x,t)|_{x=L} = \mathrm{F}R_L d_x\lambda_L. \tag{54}$$

In Eqs. (53 and 54), $\mathrm{F}R_0$ and $\mathrm{F}R_L$ represent the stiffnesses of the rotational springs at the $x=0$ and $x=L$ ends of the rotationally restrained CNTR-NW/NB, respectively. Also, if the material length scale parameter is neglected in the above expressions, the force boundary conditions in the classical elasticity theory are written as follows:

$$-\kappa_{11}\partial_{xx}v(x,t)|_{x=0} = -\mathrm{F}R_0 d_x\lambda_0, \tag{55}$$

$$-\kappa_{11}\partial_{xx}v(x,t)|_{x=L} = \mathrm{F}R_L d_x\lambda_L. \tag{56}$$

Solving Eqs. (53 and 54) yields the following two sets of equations depending on $d_{xx}\lambda_0$ and $d_{xx}\lambda_L$:

$$\left(\kappa_{11}+\kappa_{55}l^2+\sum_{n=1}^{\infty}\frac{2Ln^2\pi^2\left(\kappa_{11}+\kappa_{55}l^2\right)\mathrm{F}R_0}{\left(\kappa_{11}+\kappa_{55}l^2\right)n^4\pi^4-L^2\left(L^2M_0+n^2\pi^2M_2\right)\omega^2}\right)d_{xx}\lambda_0 + \left(-\sum_{n=1}^{\infty}\frac{2(-1)^nLn^2\pi^2\left(\kappa_{11}+\kappa_{55}l^2\right)\mathrm{F}R_0}{\left(\kappa_{11}+\kappa_{55}l^2\right)n^4\pi^4-L^2\left(L^2M_0+n^2\pi^2M_2\right)\omega^2}\right)d_{xx}\lambda_L=0. \tag{57}$$

$$\left(-\sum_{n=1}^{\infty}\frac{2(-1)^nLn^2\pi^2\left(\kappa_{11}+\kappa_{55}l^2\right)\mathrm{F}R_L}{\left(\kappa_{11}+\kappa_{55}l^2\right)n^4\pi^4-L^2\left(L^2M_0+n^2\pi^2M_2\right)\omega^2}\right)d_{xx}\lambda_0 + \left(\kappa_{11}+\kappa_{55}l^2+\sum_{n=1}^{\infty}\frac{2Ln^2\pi^2\left(\kappa_{11}+\kappa_{55}l^2\right)\mathrm{F}R_L}{\left(\kappa_{11}+\kappa_{55}l^2\right)n^4\pi^4-L^2\left(L^2M_0+n^2\pi^2M_2\right)\omega^2}\right)d_{xx}\lambda_L=0. \tag{58}$$

The above system of two equations can be conveniently written as an eigenvalue problem as follows:

$$\begin{bmatrix}\Theta_{11}^{\mathrm{RRNWB}} & \Theta_{12W}^{\mathrm{RRNWB}}\\ \Theta_{21}^{\mathrm{RRNWB}} & \Theta_{22}^{\mathrm{RRNWB}}\end{bmatrix}\begin{bmatrix}d_{xx}\lambda_0\\ d_{xx}\lambda_L\end{bmatrix}=0. \tag{59}$$

In the eigenvalue problem in Eq. (59), $\left[\Theta_{fg}^{\mathrm{RRNWB}}\right](f,g=1,2)$ is the coefficients matrix, and the eigenvalues found by setting the determinant of this coefficients matrix equal to zero ($\left|\Theta_{fg}^{\mathrm{RRNWB}}\right|=0$) give us the rotationally restrained CNTR-NW/NB. The elements of the coefficients metric are defined as follows:

$$\Theta_{11}^{\mathrm{RRNWB}}=\kappa_{11}+\kappa_{55}l^2+\sum_{n=1}^{\infty}\frac{2Ln^2\pi^2\left(\kappa_{11}+\kappa_{55}l^2\right)\mathrm{F}R_0}{\left(\kappa_{11}+\kappa_{55}l^2\right)n^4\pi^4-L^2\left(L^2M_0+n^2\pi^2M_2\right)\omega^2}. \tag{60}$$

$$\Theta_{12}^{\mathrm{RRNWB}}=-\sum_{n=1}^{\infty}\frac{2(-1)^nLn^2\pi^2\left(\kappa_{11}+\kappa_{55}l^2\right)\mathrm{F}R_0}{\left(\kappa_{11}+\kappa_{55}l^2\right)n^4\pi^4-L^2\left(L^2M_0+n^2\pi^2M_2\right)\omega^2}. \tag{61}$$

$$\Theta_{21}^{\mathrm{RRNWB}}=-\sum_{n=1}^{\infty}\frac{2(-1)^nLn^2\pi^2\left(\kappa_{11}+\kappa_{55}l^2\right)\mathrm{F}R_L}{\left(\kappa_{11}+\kappa_{55}l^2\right)n^4\pi^4-L^2\left(L^2M_0+n^2\pi^2M_2\right)\omega^2}. \tag{62}$$

$$\Theta_{22}^{\mathrm{RRNWB}}=\kappa_{11}+\kappa_{55}l^2+\sum_{n=1}^{\infty}\frac{2Ln^2\pi^2\left(\kappa_{11}+\kappa_{55}l^2\right)\mathrm{F}R_L}{\left(\kappa_{11}+\kappa_{55}l^2\right)n^4\pi^4-L^2\left(L^2M_0+n^2\pi^2M_2\right)\omega^2}. \tag{63}$$

It should also be noted that the following expression can be solved to find the results for the rotationally restrained classical wire/beam:

$$\begin{vmatrix}\Theta_{11}^{\mathrm{RRCWB}} & \Theta_{12}^{\mathrm{RRCWB}}\\ \Theta_{21}^{\mathrm{RRCWB}} & \Theta_{22}^{\mathrm{RRCWB}}\end{vmatrix}=0. \tag{64}$$

The elements of the above expression given for the classical wire/beam are written as follows:

$$\Theta_{11}^{\mathrm{RRCWB}}=\kappa_{11}+\sum_{n=1}^{\infty}\frac{2Ln^2\pi^2\kappa_{11}\mathrm{F}R_0}{\kappa_{11}n^4\pi^4-L^2\left(L^2M_0+n^2\pi^2M_2\right)\omega^2}, \tag{65}$$

$$\Theta_{12}^{\mathrm{RRCWB}}=-\sum_{n=1}^{\infty}\frac{2(-1)^nLn^2\pi^2\kappa_{11}\mathrm{F}R_0}{\kappa_{11}n^4\pi^4-L^2\left(L^2M_0+n^2\pi^2M_2\right)\omega^2}, \tag{66}$$

$$\Theta_{21}^{\mathrm{RRCWB}}=-\sum_{n=1}^{\infty}\frac{2(-1)^nLn^2\pi^2\kappa_{11}\mathrm{F}R_L}{\kappa_{11}n^4\pi^4-L^2\left(L^2M_0+n^2\pi^2M_2\right)\omega^2}, \tag{67}$$

$$\Theta_{22}^{\mathrm{RRCWB}}=\kappa_{11}+\sum_{n=1}^{\infty}\frac{2Ln^2\pi^2\kappa_{11}\mathrm{F}R_L}{\kappa_{11}n^4\pi^4-L^2\left(L^2M_0+n^2\pi^2M_2\right)\omega^2}. \tag{68}$$

The force boundary conditions associated with the shear force for the laterally restrained CNTR-NW/NB given in Fig. 4 are expressed as follows:

$$M_2\partial_{xtt}v(x,t)-\kappa_{11}\partial_{xxx}v(x,t)-\kappa_{55}l^2\partial_{xxx}v(x,t)|_{x=0}=\mathrm{F}L_0\lambda_0, \tag{69}$$

$$M_2\partial_{xtt}v(x,t)-\kappa_{11}\partial_{xxx}v(x,t)-\kappa_{55}l^2\partial_{xxx}v(x,t)|_{x=L}=-\mathrm{F}L_Ld_x\lambda_L. \tag{70}$$

In Eqs. (69 and 70), $\mathrm{F}L_0$ and $\mathrm{F}L_L$ represent the stiffness of the lateral springs at the $x=0$ and $x=L$ ends of the laterally restrained CNTR-NW/NB, respectively. Moreover, if the size parameter is neglected in the above equations, the force boundary condition of the laterally restrained classical beam analyzed by classical elasticity theory is written as follows:

$$M_2\partial_{xtt}v(x,t)-\kappa_{11}\partial_{xxx}v(x,t)|_{x=0}=\mathrm{F}L_0\lambda_0, \tag{71}$$

$$M_2\partial_{xtt}v(x,t)-\kappa_{11}\partial_{xxx}v(x,t)|_{x=L}=-\mathrm{F}L_L\lambda_L. \tag{72}$$

By solving Eqs. (71 and 72), the following two sets of equations related to λ_0 and λ_L are obtained:

$$\left(-\mathrm{F}L_0+\frac{M_2\omega^2}{L}+\sum_{n=1}^{\infty}\frac{2LM_0\omega^2\left(-\kappa_{11}n^2\pi^2+L^2M_2\omega^2-\kappa_{55}l^2n^2\pi^2\right)}{L^4M_0\omega^2+L^2n^2\pi^2M_2\omega^2-\left(\kappa_{11}+\kappa_{55}l^2\right)n^4\pi^4}\right)\lambda_0 + \left(-\frac{M_2\omega^2}{L}-\sum_{n=1}^{\infty}\frac{2(-1)^nLM_0\omega^2\left(-\kappa_{11}n^2\pi^2+L^2M_2\omega^2-\kappa_{55}l^2n^2\pi^2\right)}{L^4M_0\omega^2+L^2n^2\pi^2M_2\omega^2-\left(\kappa_{11}+\kappa_{55}l^2\right)n^4\pi^4}\right)\lambda_L=0. \tag{73}$$

$$\left(-\frac{M_2\omega^2}{L}-\sum_{n=1}^{\infty}\frac{2(-1)^nLM_0\omega^2\left(-\kappa_{11}n^2\pi^2+L^2M_2\omega^2-\kappa_{55}l^2n^2\pi^2\right)}{L^4M_0\omega^2+L^2n^2\pi^2M_2\omega^2-\left(\kappa_{11}+\kappa_{55}l^2\right)n^4\pi^4}\right)\lambda_0 + \left(-\mathrm{F}L_L+\frac{M_2\omega^2}{L}+\sum_{n=1}^{\infty}\frac{2LM_0\omega^2\left(-\kappa_{11}n^2\pi^2+L^2M_2\omega^2-\kappa_{55}l^2n^2\pi^2\right)}{L^4M_0\omega^2+L^2n^2\pi^2M_2\omega^2-\left(\kappa_{11}+\kappa_{55}l^2\right)n^4\pi^4}\right)\lambda_L=0. \tag{74}$$

Equations (73 and 74) can be written as an eigenvalue problem as follows:

$$\begin{bmatrix} \Theta_{11}^{TTNWB} & \Theta_{12}^{TTNWB} \\ \Theta_{21}^{TTNWB} & \Theta_{22}^{TTNWB} \end{bmatrix} \begin{bmatrix} \lambda_0 \\ \lambda_L \end{bmatrix} = 0. \tag{75}$$

In the eigenvalue problem in Eq. (75), $[\Theta_{fg}^{\mathrm{TTNWB}}]$ $(f, g = 1,2)$ is the coefficients matrix that gives the solution of the laterally restrained CNTR-NW/NB and is found by setting the determinant of this coefficient matrix equal to zero ($|\Theta_{fg}^{\mathrm{TTNWB}}|=0$). The eigenvalues give us the free vibration frequencies of the laterally restrained CNTR-NW/NB. The elements of the mentioned coefficients matrix are defined as follows:

$$\Theta_{11}^{\mathrm{TTNWB}} = -\mathrm{F}L_0 + \frac{M_2\omega^2}{L} + \sum_{n=1}^{\infty} \frac{2LM_0\omega^2\left(-\kappa_{11}n^2\pi^2 + L^2M_2\omega^2 - \kappa_{55}l^2n^2\pi^2\right)}{L^4M_0\omega^2 + L^2n^2\pi^2M_2\omega^2 - \left(\kappa_{11} + \kappa_{55}l^2\right)n^4\pi^4}, \tag{76}$$

$$\Theta_{12}^{\mathrm{TTNWB}} = -\frac{M_2\omega^2}{L} - \sum_{n=1}^{\infty} \frac{2(-1)^nLM_0\omega^2\left(-\kappa_{11}n^2\pi^2 + L^2M_2\omega^2 - \kappa_{55}l^2n^2\pi^2\right)}{L^4M_0\omega^2 + L^2n^2\pi^2M_2\omega^2 - \left(\kappa_{11} + \kappa_{55}l^2\right)n^4\pi^4}, \tag{77}$$

$$\Theta_{21}^{\mathrm{TTNWB}} = -\frac{M_2\omega^2}{L} - \sum_{n=1}^{\infty} \frac{2(-1)^nLM_0\omega^2\left(-\kappa_{11}n^2\pi^2 + L^2M_2\omega^2 - \kappa_{55}l^2n^2\pi^2\right)}{L^4M_0\omega^2 + L^2n^2\pi^2M_2\omega^2 - \left(\kappa_{11} + \kappa_{55}l^2\right)n^4\pi^4}, \tag{78}$$

$$\Theta_{22}^{\mathrm{TTNWB}} = -\mathrm{F}L_L + \frac{M_2\omega^2}{L} + \sum_{n=1}^{\infty} \frac{2LM_0\omega^2\left(-\kappa_{11}n^2\pi^2 + L^2M_2\omega^2 - \kappa_{55}l^2n^2\pi^2\right)}{L^4M_0\omega^2 + L^2n^2\pi^2M_2\omega^2 - \left(\kappa_{11} + \kappa_{55}l^2\right)n^4\pi^4}. \tag{79}$$

It should also be noted that the following expression can be solved to find the results for the laterally restrained classical beam/wire:

$$\begin{vmatrix} \Theta_{11}^{\mathrm{TTCWB}} & \Theta_{12}^{\mathrm{TTCWB}} \\ \Theta_{21}^{\mathrm{TTCWB}} & \Theta_{22}^{\mathrm{TTCWB}} \end{vmatrix} = 0. \tag{80}$$

The elements of the above expression given for the classical beam/wire are written as follows:

$$\Theta_{11}^{\mathrm{TTCWB}} = -\mathrm{F}L_0 + \frac{M_2\omega^2}{L} + \sum_{n=1}^{\infty} \frac{2LM_0\omega^2\left(-\kappa_{11}n^2\pi^2 + L^2M_2\omega^2\right)}{-\kappa_{11}n^4\pi^4 + L^4M_0\omega^2 + L^2n^2\pi^2M_2\omega^2}, \tag{81}$$

$$\Theta_{12}^{\mathrm{TTCWB}} = -\frac{M_2\omega^2}{L} - \sum_{n=1}^{\infty} \frac{2(-1)^nLM_0\omega^2\left(-\kappa_{11}n^2\pi^2 + L^2M_2\omega^2\right)}{-\kappa_{11}n^4\pi^4 + L^4M_0\omega^2 + L^2n^2\pi^2M_2\omega^2}, \tag{82}$$

$$\Theta_{21}^{\mathrm{TTCWB}} = -\frac{M_2\omega^2}{L} - \sum_{n=1}^{\infty} \frac{2(-1)^nLM_0\omega^2\left(-\kappa_{11}n^2\pi^2 + L^2M_2\omega^2\right)}{-\kappa_{11}n^4\pi^4 + L^4M_0\omega^2 + L^2n^2\pi^2M_2\omega^2}, \tag{83}$$

$$\Theta_{22}^{\mathrm{TTCWB}} = -\mathrm{F}L_L + \frac{M_2\omega^2}{L} + \sum_{n=1}^{\infty} \frac{2LM_0\omega^2\left(-\kappa_{11}n^2\pi^2 + L^2M_2\omega^2\right)}{-\kappa_{11}n^4\pi^4 + L^4M_0\omega^2 + L^2n^2\pi^2M_2\omega^2}. \tag{84}$$

It is necessary to explain several important points, the two models of which will be analyzed. As can be seen in the model given in Fig. 3, CNTR-NW/NB, which sits on simply supports, is restricted by rotational springs. While these rotational spring stiffnesses can be so small that they are almost ineffective, they can also have such large stiffness that they prevent rotation. In these cases, the rigid conditions of simply supported and clamped at both ends are met, respectively. In other words, rotationally restrained CNTR-NW/NB can meet the SS and CC boundary conditions and the situations between them by adjusting the rotational spring stiffness. As can be seen in the model given in Fig. 4, the CNTR-NW/NB is on the lateral springs at its ends. The stiffness of these lateral springs can have a stiffness so small that they are almost ineffective, but they can also have a stiffness large enough to prevent deflection. In these cases, two free ends and simply supported rigid conditions are met, respectively. In other words, laterally restrained CNTR-NW/NB can meet the free-free at both ends (FF) and SS boundary conditions and the states in between by adjusting the lateral spring stiffness. Also, a flowchart for the methodology used in this work is shown via Fig. 5.

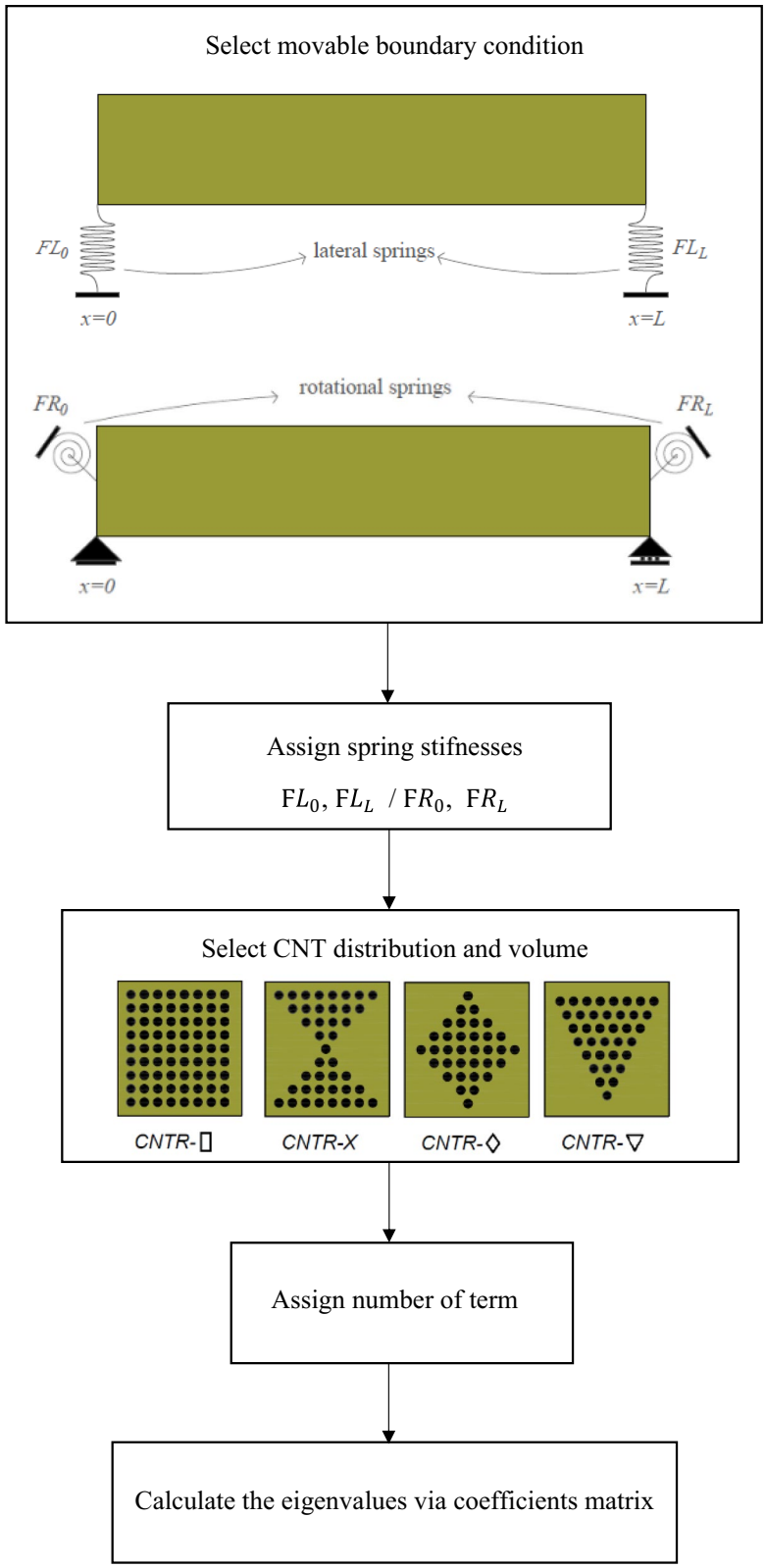


Fig. 5 Flowchart for the methodology used in this work

Analyses for CNTR-NW/NB

In this section, free vibration analysis of carbon nanotube-reinforced composite rectangular NWs/NBs will be carried out. Unless stated otherwise, the properties used for the materials forming the carbon nanotube-reinforced composite NWs/NBs are as follows [15]: $E^{\mathrm{PMMA}} = 2.5\mathrm{GPa}$, $\upsilon^{\mathrm{PMMA}} = 0.3$, $\rho^{\mathrm{PMMA}} = 1190\mathrm{kg/m^3}$, $E_{11}^{\mathrm{CNT}} = 600\mathrm{GPa}$, $E_{22}^{\mathrm{CNT}} = 10\mathrm{GPa}$, $G_{12}^{\mathrm{CNT}} = 17.2\mathrm{GPa}$, $\upsilon^{\mathrm{CNT}} = 0.19$, $\rho^{\mathrm{CNT}} = 1400\mathrm{kg/m^3}$. Additionally, $b = 10$ nm, $h = 2b = 20$ nm and $L = 20\ h = 400$ nm are taken. In the study, some dimensionless parameters are used for CNTR-NWs/NBs. The parameters in the dimensionless form used are as follows [15]:

$$\overline{\omega} = \omega L \sqrt{\frac{b\int_{-\frac{h}{2}}^{+\frac{h}{2}} \rho^{\mathrm{PMMA}} dz}{b\int_{-\frac{h}{2}}^{+\frac{h}{2}} E^{\mathrm{PMMA}} dz}}, \tag{85}$$

$$\overline{\mathrm{F}R_0} = \frac{\mathrm{F}R_0 L}{b\int_{-\frac{h}{2}}^{+\frac{h}{2}} E^{\mathrm{PMMA}} z^2 dz}, \tag{86}$$

$$\overline{\mathrm{F}R_L} = \frac{\mathrm{F}R_L L}{b\int_{-\frac{h}{2}}^{+\frac{h}{2}} E^{\mathrm{PMMA}} z^2 dz}, \tag{87}$$

$$\overline{\mathrm{F}L_0} = \frac{\mathrm{F}L_0 L}{b\int_{-\frac{h}{2}}^{+\frac{h}{2}} E^{\mathrm{PMMA}} dz}, \tag{88}$$

$$\overline{\mathrm{F}L_L} = \frac{\mathrm{F}L_L L}{b\int_{-\frac{h}{2}}^{+\frac{h}{2}} E^{\mathrm{PMMA}} dz}. \tag{89}$$

This study is based on the solution of an eigenvalue problem containing infinite series of elements. To provide the solution, the infinite series must be cut at a certain term and the frequencies obtained accordingly. The number of terms can be low or high depending on the boundary condition. We can decide the optimum number of terms by comparisons with some studies in the literature. In Table 1, the dimensionless vibration frequencies of CNTR beams based on the MCST are compared with the study presented by Civalek et al. [45] for RB and EBB theories. For this comparison, $l = h$ is taken and additionally, $L/h = 15$. In this comparison, the number of terms is selected as 30 ($n = 30$), and it should be noted that this number of terms is low. Using a low number of terms also reduces solution time. As can be seen, excellent agreement is achieved at dimensionless frequencies based on the MCST. It is worth noting here that, unless a special situation is stated, the

Table 1 Comparison of dimensionless frequencies of CNTR small-scale beams based on MCST (CNTR-□, SS)

Beam theory	Ref. [45]	This study $\overline{\mathrm{F}L_0} = \overline{\mathrm{F}L_L} = 10^{10}$	This study $\overline{\mathrm{F}R_0} = \overline{\mathrm{F}R_L} = 10^{-10}$
$\Xi^*_{\mathrm{CNT}} = 0.12$			
EBB	1.2256	1.22564	1.22564
RB	1.2234	1.2234	1.2234
$\Xi^*_{\mathrm{CNT}} = 0.17$			
EBB	1.4909	1.49089	1.49089
RB	1.4882	1.48817	1.48817

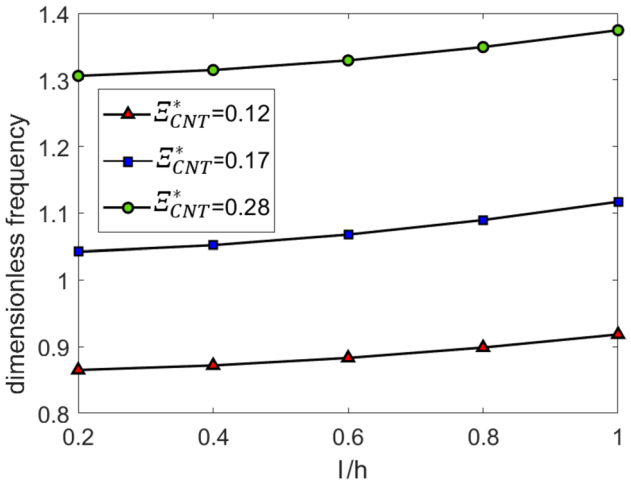


Fig. 6 Dimensionless frequencies of CNTR-□ versus l/h

Table 2 Comparison of dimensionless frequencies of homogeneous small-scale beams based on MCST (EBB, CC)

This study $\overline{\mathrm{F}R_0} = \overline{\mathrm{F}R_L} = 10^{10}$					Difference (%)	Ref. [31]
$n=30$	$n=50$	$n=70$	$n=90$	$n=110$	0.747246	27.2467
28.0227	27.7025	27.5693	27.4964	27.4503		
$n=40$	$n=60$	$n=80$	$n=100$	$n=120$	0.68412	
27.821	27.6245	27.5282	27.471	27.4331		

analyzes in this study are carried out with $n = 30$ and the spring parameters used in Table 1.

In Table 2, a comparison is made for a homogeneous microbeam clamped at both ends. The aim here is to determine the number of terms required to satisfy or to converge sufficiently the clamped boundary condition. The comparison study in Table 2 is carried out with the frequencies calculated by Toğun and Bağdatlı [31] with the perturbation method. In this comparison for the first vibration mode, the number of terms started from 30 and is cut off at 120. The parameters used in this comparison are as follows: $E = 1.44$ GPa, $\rho = 1220$ kg/m^3, $\upsilon = 0.38$. It is clear that by increasing the number of terms, the calculated frequencies approach those calculated by Togun and Bağdatlı [31] and the difference decreases. The difference is calculated by:

$$\text{Difference} = \frac{\text{frequency calculated by Eq. (59)} - \text{frequency calculated by Ref.[31]}}{\text{frequency calculated by Ref.[31]}} \times 100. \tag{90}$$

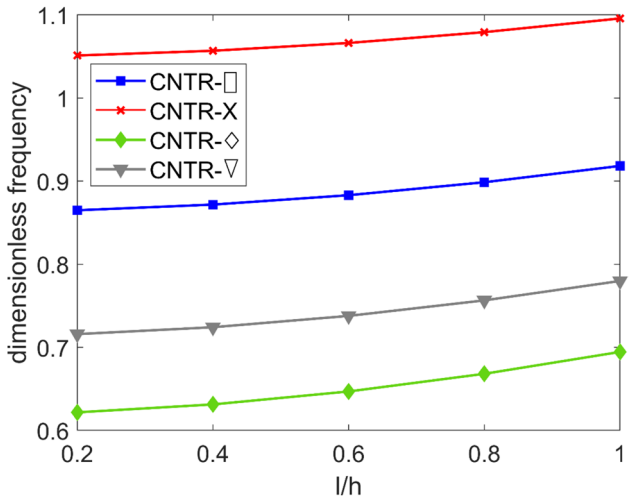


Fig. 7 Dimensionless frequencies of CNTR-NWs/NBs versus l/h

In Fig. 6, the dimensionless frequencies of CNTR-□ according to varying l/h are plotted for three different Ξ^*_{CNT} values. In this example, RB theory is considered. The increase in dimensionless frequencies with increasing l and Ξ^*_{CNT} can be easily observed here as well. What is really emphasized here is the effect of l and Ξ^*_{CNT}. When l/h is increased, the highest increase in dimensionless frequencies is calculated for $\Xi^*_{CNT} = 0.17$. On the other hand, the lowest increase ratio is obtained for $\Xi^*_{CNT} = 0.28$.

In Fig. 7, the effect of material length scale parameter is plotted for composite nanowires/nanobeams with different CNT distributions. The frequency-increasing effect of l is clearly seen here as well. The point to emphasize here is in which distribution the material length scale parameter is more effective. It is clear from the figure that as l/h increases, the increase in the frequencies of CNTR-◇ is sharper. The nanowire/nanobeam least affected by the increase of l/h is CNTR-X.

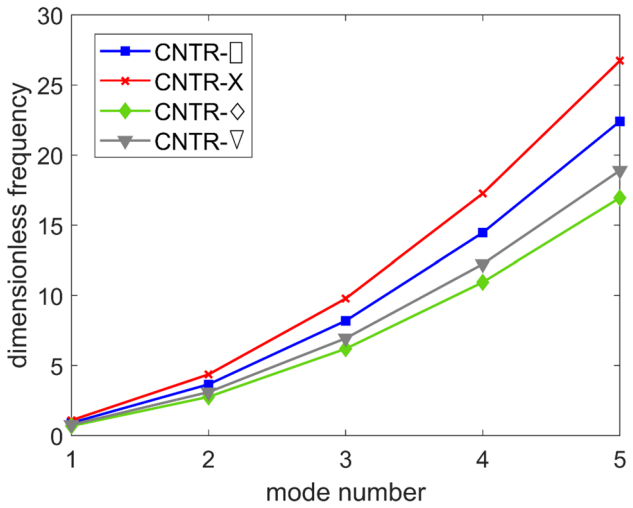


Fig. 8 Dimensionless frequencies of CNTR-NWs/NBs versus mode number

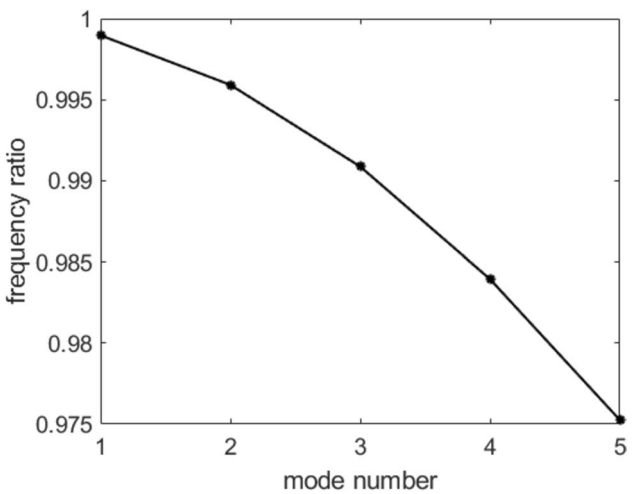


Fig. 9 Frequency ratios of CNTR-□ versus mode number

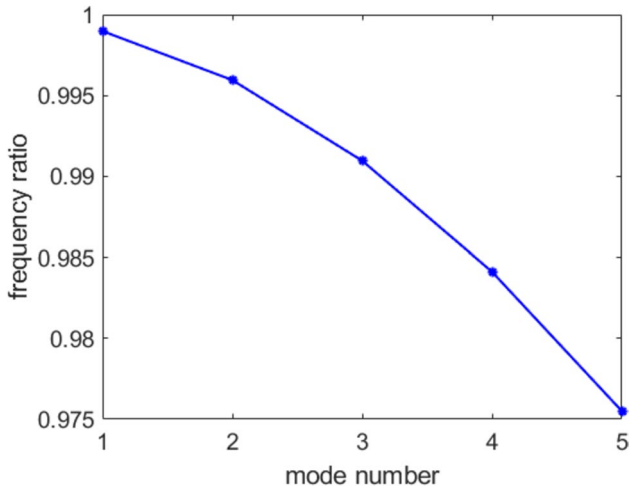


Fig. 10 Frequency ratios of CNTR-◊ versus mode number

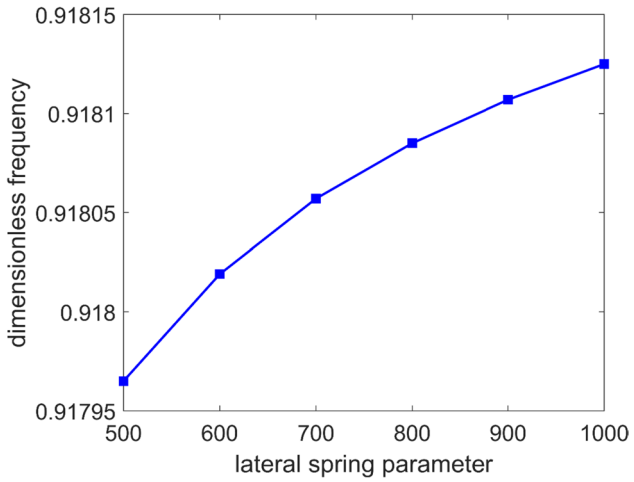


Fig. 11 Dimensionless frequencies of CNTR-□ versus lateral spring parameter

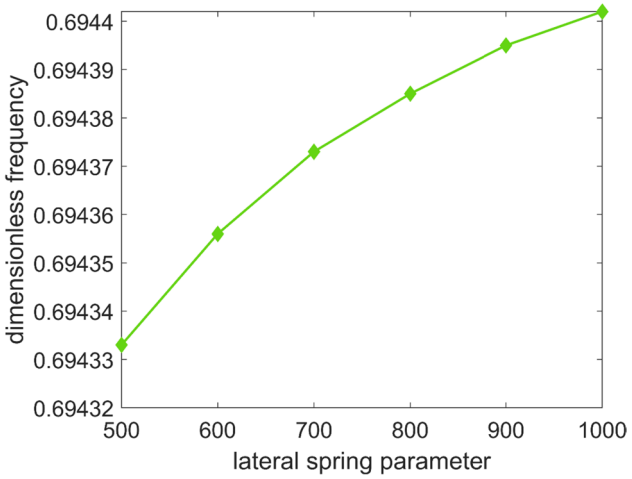


Fig. 12 Dimensionless frequencies of CNTR-◊ versus lateral spring parameter

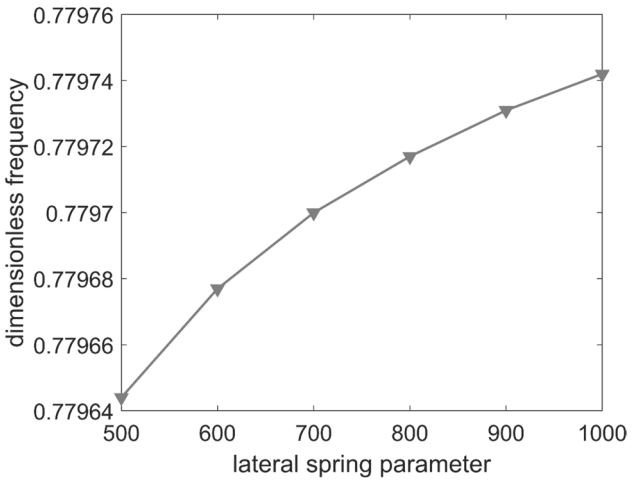


Fig. 13 Dimensionless frequencies of CNTR-▽ versus lateral spring parameter

In Fig. 8, a comparison of dimensionless frequencies based on MCST and RB theory is made for various CNT distributions. For this example, $\Xi^*_{CNT} = 0.12$ and $l = h$. It should also be noted that unless otherwise stated, $l = h$ is used in the analyses. From this figure drawn for the first five vibration modes, it can be seen that the highest frequencies are obtained for CNTR-X and the lowest frequencies are obtained for CNTR-◊.

Figures 9 and 10 are drawn to emphasize the effect of rotary inertia. As known, the difference between Euler–Bernoulli and Rayleigh beam theories is the rotary inertia effect. While Rayleigh beam theory takes into account the rotary inertia effect, Euler–Bernoulli beam theory is independent of the rotary inertia effect. Since the consideration of the rotary inertia effect affects the frequencies in a small amount, its analysis is carried out on frequency ratios. The frequency ratios stated in the figures are defined as RB/EBB and are calculated for $\Xi^*_{CNT} = 0.12$, $l = h$. Since the frequency values calculated with RB theory are lower, the frequency ratios take values below 1, and as can be understood, the frequency ratio decreases as the mode number increases. From this, it is understood that the effect of rotary inertia is more evident in higher modes.

The originality of this study is that it offers solutions that can examine the frequencies of CNTR-NW/NBs in movable boundary conditions. In Figs. 11, 12, 13, the effect of springs capable of lateral motion on the frequencies of CNTR-◊, CNTR-□ and CNTR-▽ is examined for the first mode. For

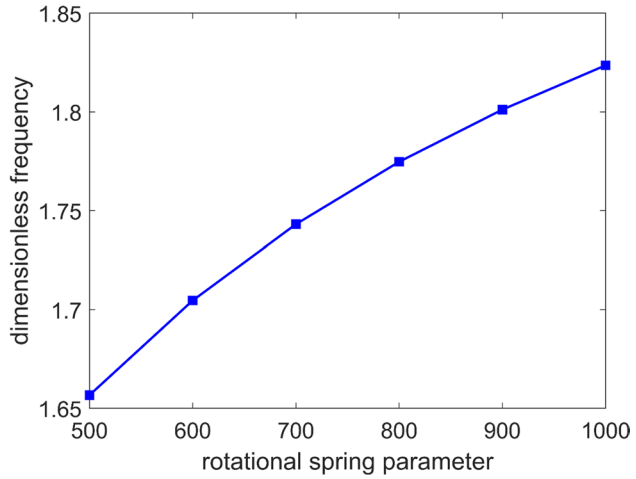


Fig. 14 Dimensionless frequencies of CNTR-□ versus rotational spring parameter

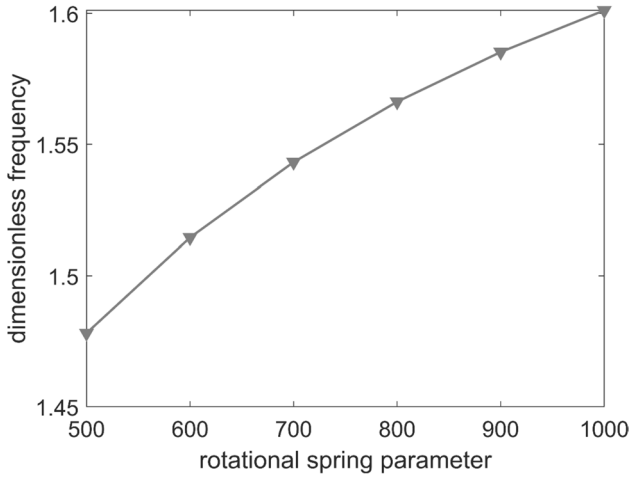


Fig. 16 Dimensionless frequencies of CNTR-▽ versus rotational spring parameter

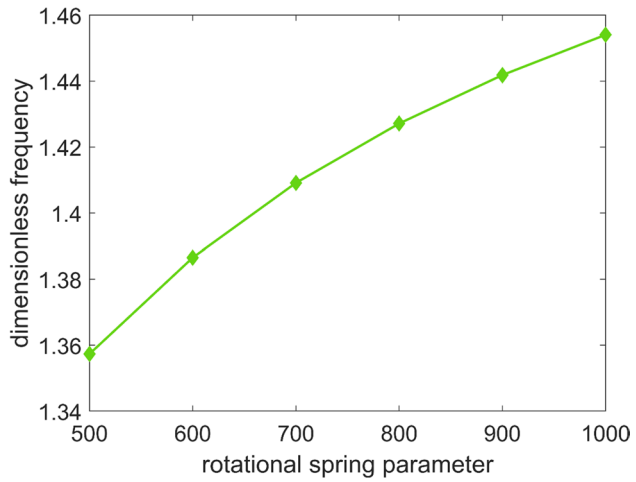


Fig. 15 Dimensionless frequencies of CNTR-◇ versus rotational spring parameter

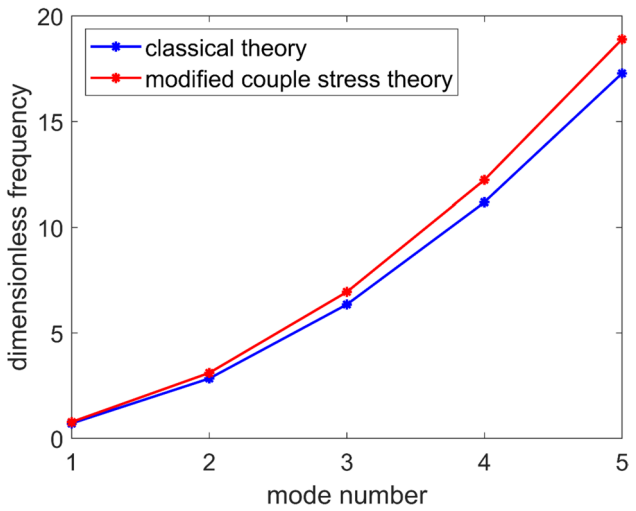


Fig. 17 Dimensionless frequencies for different theories

these examples, lateral spring parameter (dimensionless lateral spring stiffness) values are considered as six different values: $\overline{FL_0} = \overline{FL_L} = 500, 600, 700, 800, 900, 1000$. In the figures examining the effect of spring parameters, the carbon nanotube volume fraction is 0.12, $l = h$ and $n = 100$. It is clear from these graphs that increasing spring stiffness causes the frequencies to increase. As mentioned before, the stiffness of these springs can be taken at numerous values, from zero to infinitely large. This demonstrates the solution method's ability to examine numerous combinations that can occur in boundary conditions.

In Figs. 14, 15, 16, the effect of rotational springs is analyzed. Six different values for rotational spring parameters (dimensionless rotational spring stiffness) are chosen and the frequencies of the CNTR nanobeams in the previous example are plotted. Increasing the stiffness of the rotational springs results in an increase of the dimensionless frequencies.

Finally, in Fig. 17, the effect of the size-dependent theory, MCST, is analyzed. For this example, $\Xi^*_{\mathrm{CNT}} = 0.12$ is chosen and the properties of CNTR-▽ are used. In this example, where the effect of rotary inertia is also considered, the variation of frequencies for the first five mode is shown. We can easily see that the classical theory has lower frequencies. It is worth noting again that we can obtain the results of the classical theory when we set the length scale parameter to zero in the solution given for MCST.

Conclusions

In this study, the vibration analysis of a nanowire/nanobeam reinforced with carbon nanotubes is carried out under movable boundary conditions. The cross section of the nanobeam is assumed to be rectangular and four different carbon nanotube reinforcement distribution configurations are applied. Laterally deformable springs and rotational springs are used at the ends to ensure generality in boundary conditions. Fourier sine series is chosen as the analytical displacement function and the degrees of freedom at the end points are separated from the region and these points are defined separately. Stokes' transformation is applied to incorporate the separately defined values in these regions into the problem and eigenvalue problems governing the vibration of carbon nanotube-reinforced nanowires/nanobeams are obtained. Then, a series of numerical examples are solved and the effects of carbon nanotube distribution, material length scale parameter, rotary inertia, carbon nanotube volume fraction, lateral spring parameter and rotational spring parameter on the vibration frequencies are analyzed with a series of graphs after validation with studies in the literature. The main outcomes of the studies can be summarized as follows: increasing the volume fraction of the carbon nanotube, which is used as the matrix-reinforcing element, increases the frequencies of the composite nanowire/nanobeam. It is understood that the carbon nanotube distribution type is very effective on the frequencies of the composite nanowire/nanobeam. The highest frequencies are obtained for CNTR-X, while the lowest frequencies are calculated for CNTR-◇. It should be noted that the frequencies increase with the increase of the material length scale parameter. While increasing the stiffness of the deformable springs at both ends of the reinforced composite nanowires/nanobeams causes an increase in the frequencies, addressing the rotary inertia effect reduces the frequencies.

Funding Open access funding provided by the Scientific and Technological Research Council of Türkiye (TÜBİTAK).

Declarations

Conflict of Interest No potential conflict of interest was reported by the authors.

Open Access This article is licensed under a Creative Commons Attribution 4.0 International License, which permits use, sharing, adaptation, distribution and reproduction in any medium or format, as long as you give appropriate credit to the original author(s) and the source, provide a link to the Creative Commons licence, and indicate if changes were made. The images or other third party material in this article are included in the article's Creative Commons licence, unless indicated otherwise in a credit line to the material. If material is not included in the article's Creative Commons licence and your intended use is not permitted by statutory regulation or exceeds the permitted use, you will need to obtain permission directly from the copyright holder. To view a copy of this licence, visit http://creativecommons.org/licenses/by/4.0/.

References

1. Bakhshi Khaniki H, Hosseini-Hashemi S (2017) Dynamic transverse vibration characteristics of nonuniform nonlocal strain gradient beams using the generalized differential quadrature method. Eur Phys J Plus 132:1–15
2. Esen İ, Koç MA, Eroğlu M (2023) Effect of functionally graded carbon nanotube reinforcement on the dynamic response of composite beams subjected to a moving charge. J Vib Eng Technol. https://doi.org/10.1007/s42417-023-01192-0
3. Mahmoodi SN, Khadem SE, Jalili N (2006) Theoretical development and closed-form solution of nonlinear vibrations of a directly excited nanotube-reinforced composite cantilever beam. Arch Appl Mech 75(2):153–163. https://doi.org/10.1007/s00419-005-0426-1
4. Lin F, Xiang Y (2014) Vibration of carbon nanotube reinforced composite beams based on the first and third order beam theories. Appl Math Model 38(15–16):3741–3754. https://doi.org/10.1016/j.apm.2014.02.008
5. Heshmati M, Yas MH, Daneshmand F (2015) A comprehensive study on the vibrational behavior of CNT-reinforced composite beams. Compos Struct 125:434–448. https://doi.org/10.1016/j.compstruct.2015.02.033
6. Rafiee M, Yang J, Kitipornchai S (2013) Large amplitude vibration of carbon nanotube reinforced functionally graded composite beams with piezoelectric layers. Compos Struct 96:716–725. https://doi.org/10.1016/j.compstruct.2012.10.005
7. Zhang W, He LJ, Wang JF (2022) Content-dependent nonlinear vibration of composite plates reinforced with carbon nanotubes. J Vib Eng Technol 10(4):1253–1264
8. Özdemir Ö, Esen İ, Ural H (2023) Vibration response of rotating carbon nanotube reinforced composites in thermal environment. Steel Compos Struct 47(1):1–17
9. Ghandehari MA, Masoodi AR, Panda SK (2023) Thermal frequency analysis of double CNT-reinforced polymeric straight beam. J Vib Eng Technol. p 1–17.
10. Bondla S, Sharma N, Panda SK, Hirwani CK, Mahmoud SR, Kumar V (2022) Uncertain frequency responses of CNT–reinforced polymeric graded structure using fuzzified elastic properties–fuzzy finite element approach. Waves Random Complex Media. https://doi.org/10.1080/17455030.2022.2147599
11. Mehar K, Panda SK, Mahapatra TR (2018) Thermoelastic deflection responses of CNT reinforced sandwich shell structure using finite element method. Scientia Iranica 25(5):2722–2737
12. Mehar K, Kumar EK, Patle BK, Panda SK, Biswas S, Devarajan Y (2023) Thermoelastic frequency prediction of nanotube-reinforced graded smart (shape memory alloy-reinforced) sandwich structure. J Vib Eng Technol. https://doi.org/10.1007/s42417-023-01206-x
13. Mehar K, Panda SK, Sharma N (2020) Numerical investigation and experimental verification of thermal frequency of carbon nanotube-reinforced sandwich structure. Eng Struct 211:110444
14. Esen I, Tran TT, Nguyen DK (2022) Dynamic response of FG-CNTRC beams subjected to a moving mass. Vietnam J Sci Technol 60(5):853–868
15. Wattanasakulpong N, Ungbhakorn V (2013) Analytical solutions for bending, buckling and vibration responses of carbon nanotube-reinforced composite beams resting on elastic foundation. Comput Mater Sci 71:201–208

16. Ke LL, Yang J, Kitipornchai S (2010) Nonlinear free vibration of functionally graded carbon nanotube-reinforced composite beams. Compos Struct 92(3):676–683
17. Wu HL, Yang J, Kitipornchai S (2016) Nonlinear vibration of functionally graded carbon nanotube-reinforced composite beams with geometric imperfections. Compos B Eng 90:86–96
18. Alimoradzadeh M, Akbas SD (2023) Nonlinear vibration analysis of carbon nanotube-reinforced composite beams resting on nonlinear viscoelastic foundation. Geomech Eng 32(2):125–135
19. Mehar K, Panda SK, Mahapatra TR (2017) Theoretical and experimental investigation of vibration characteristic of carbon nanotube reinforced polymer composite structure. Int J Mech Sci 133:319–329
20. Satankar RK, Sharma N, Katariya PV, Kumar V, Dewangan HC, Pal A, Panda SK (2023) Computational modelling and analysis of thermoacoustic behaviour of carbon nanotube-reinforced plant fibre epoxy composite–an extensive review. Mater Today Commun. 36:106717
21. Liew KM, Lei ZX, Zhang LW (2015) Mechanical analysis of functionally graded carbon nanotube reinforced composites: a review. Compos Struct 120:90–97
22. Yang FACM, Chong ACM, Lam DCC, Tong P (2002) Couple stress based strain gradient theory for elasticity. Int J Solids Struct 39(10):2731–2743
23. Eringen AC (1972) Nonlocal polar elastic continua. Int J Eng Sci 10(1):1–16
24. Toupin RA (1964) Theories of elasticity with couple-stress. Arch Ration Mech Anal 17:85–112
25. Koiter WT (1946) Couple stresses in the theory of elasticity. Proc Koninklijke Nederl Akaad van Wetensch. 67.
26. Granik VT, Ferrari M (1993) Microstructural mechanics of granular media. Mech Mater 15(4):301–322
27. Ferrari M, Granik VT, Imam A, Nadeau JC (2008) Advances in doublet mechanics, vol 45. Springer Science & Business Media, New York
28. Lam DCC, Yang F, Chong ACM, Wang J, Tong P (2003) Experiments and theory in strain gradient elasticity. J Mech Phys Solids 51:1477–1508
29. Lim CW, Zhang G, Reddy J (2015) A higher-order nonlocal elasticity and strain gradient theory and its applications in wave propagation. J Mech Phys Solids 78:298–313
30. Ersoy H, Civalek Ö, Numanoğlu HM, Akgöz B (2018) Small size and rotary inertia effects on the natural frequencies of carbon nanotubes. Curved and Layered Structures 5(1):273–279
31. Togun N, Bağdatli SM (2016) Size dependent nonlinear vibration of the tensioned nanobeam based on the modified couple stress theory. Compos B Eng 97:255–262
32. Eltaher MA, Abdelrahman AA, Esen I (2021) Dynamic analysis of nanoscale Timoshenko CNTs based on doublet mechanics under moving load. The European Physical Journal Plus 136(7):705
33. Özmen R, Esen I (2023) Dynamic response of embedded Timoshenko CNTs exposed to magnetic and thermal fields subjected to moving load based on doublet mechanics. J Braz Soc Mech Sci Eng 45(11):590
34. Gul U, Aydogdu M (2021) A micro/nano-scale Timoshenko-Ehrenfest beam model for bending, buckling and vibration analyses based on doublet mechanics theory. European Journal of Mechanics-A/Solids 86:104199
35. Awrejcewicz J, Krysko VA, Pavlov SP, Zhigalov MV, Kalutsky LA, Krysko AV (2020) Thermoelastic vibrations of a Timoshenko microbeam based on the modified couple stress theory. Nonlinear Dyn 99:919–943
36. Esen I (2020) Dynamics of size-dependant Timoshenko micro beams subjected to moving loads. Int J Mech Sci 175:105501
37. Ghadiri M, Soltanpour M, Yazdi A, Safi M (2016) Studying the influence of surface effects on vibration behavior of size-dependent cracked FG Timoshenko nanobeam considering nonlocal elasticity and elastic foundation. Appl Phys A 122:1–21
38. Esen I, Özarpa C, Eltaher MA (2021) Free vibration of a cracked FG microbeam embedded in an elastic matrix and exposed to magnetic field in a thermal environment. Compos Struct 261:113552
39. Abdelrahman AA, Esen I, Ozarpa C, Shaltout R, Eltaher MA, Assie AE (2021) Dynamics of perforated higher order nanobeams subject to moving load using the nonlocal strain gradient theory. Smart Struct Syst 28(4):515–533
40. Kafkas U, Uzun B, Yaylı MÖ, Güçlü G (2023) Thermal vibration of perforated nanobeams with deformable boundary conditions via nonlocal strain gradient theory. Z Naturforsch. https://doi.org/10.1515/zna-2023-0088
41. Kafkas U, Unal Y, Yayli MO, Uzun B (2023) Buckling analysis of perforated nano/microbeams with deformable boundary conditions via nonlocal strain gradient elasticity. Advances in nano research 15(4):339–353
42. Esen I (2020) Response of a micro-capillary system exposed to a moving mass in magnetic field using nonlocal strain gradient theory. Int J Mech Sci 188:105937
43. Özarpa C, Esen I (2020) Modelling the dynamics of a nanocapillary system with a moving mass using the non-local strain gradient theory. Math Methods Appl Sci. https://doi.org/10.1002/mma.6812
44. Thai CH, Hung PT, Nguyen-Xuan H, Phung-Van P (2023) A size-dependent meshfree approach for magneto-electro-elastic functionally graded nanoplates based on nonlocal strain gradient theory. Eng Struct 292:116521
45. Civalek Ö, Dastjerdi S, Akbaş ŞD, Akgöz B (2021) Vibration analysis of carbon nanotube-reinforced composite microbeams. Math Methods Appl Sci. https://doi.org/10.1002/mma.7069
46. Alimoradzadeh M, Heidari H, Tornabene F, Dimitri R (2023) Nonlinear dynamic study of non-uniform microscale CNTR composite beams based on a modified couple stress theory. Int J Non-Linear Mech. https://doi.org/10.1016/j.ijnonlinmec.2023.104477
47. Abdelrahman AA, Esen I, Daikh AA, Eltaher MA (2023) Dynamic analysis of FG nanobeam reinforced by carbon nanotubes and resting on elastic foundation under moving load. Mech Based Des Struct Mach 51(10):5383–5406
48. Esen I, Daikh AA, Eltaher MA (2021) Dynamic response of nonlocal strain gradient FG nanobeam reinforced by carbon nanotubes under moving point load. The European Physical Journal Plus 136(4):1–22
49. Daikh AA, Bachiri A, Houari MSA, Tounsi A (2020) Size dependent free vibration and buckling of multilayered carbon nanotubes reinforced composite nanoplates in thermal environment. Mech Based Des Struct Mach. https://doi.org/10.1080/15397734.2020.1752232
50. Daikh AA, Drai A, Houari MSA, Eltaher MA (2020) Static analysis of multilayer nonlocal strain gradient nanobeam reinforced by carbon nanotubes. Steel Compos Struct Int J 36(6):643–656
51. Borjalilou V, Taati E, Ahmadian MT (2019) Bending, buckling and free vibration of nonlocal FG-carbon nanotube-reinforced composite nanobeams: exact solutions. SN Applied Sciences 1:1–15
52. Taati E, Borjalilou V, Fallah F, Ahmadian MT (2022) On size-dependent nonlinear free vibration of carbon nanotube-reinforced beams based on the nonlocal elasticity theory: Perturbation technique. Mech Based Design Struct Mach. 50(6):2124–2146
53. Shen HS (2009) Nonlinear bending of functionally graded carbon nanotube-reinforced composite plates in thermal environments. Compos Struct 91(1):9–19

54. Hu H, Onyebueke L, Abatan A (2010) Characterizing and modeling mechanical properties of nanocomposites-review and evaluation. J Min Mater Characterization Eng 9(04):275
55. Agarwal BD, Broutman LJ (1990) Analysis and performance of fber composites, 2nd edn. Wiley, New York
56. Moradi-Dastjerdi R, Foroutan A, Pourasgha AE (2012) Mori-Tanaka approach for vibrational behavior of continuously graded carbon nanotube-reinforced cylindrical panels. Compos Part B-Eng 43:1943–1954
57. Mori T, Tanaka K (1973) Average stress in matrix and average elastic energy of materials with misfitting inclusions. Acta Metall 21(5):571–574
58. Kim HK, Kim MS (2001) Vibration of beams with generally restrained boundary conditions using Fourier series. J Sound Vib 245(5):771–784
59. Civalek Ö, Uzun B, Yayli MÖ (2021) Buckling analysis of nanobeams with deformable boundaries via doublet mechanics. Arch Appl Mech 91:4765–4782
60. Civalek Ö, Ersoy H, Uzun B, Yaylı MÖ (2023) Dynamics of a FG porous microbeam with metal foam under deformable boundaries. Acta Mech 234(11):5385–5404
61. Uzun B, Kafkas U, Yaylı MÖ (2020) Stability analysis of restrained nanotubes placed in electromagnetic field. Microsyst Technol 26(12):3725–3736

Publisher's Note Springer Nature remains neutral with regard to jurisdictional claims in published maps and institutional affiliations.